Synergistic interaction between gefitinib (Iressa, ZD1839) and paclitaxel against human gastric carcinoma cells

Jong-Kook Park[a], Sang-Hak Lee[a], Jin-Hyoung Kang[b], Kazuto Nishio[c], Nagahiro Saijo[c] and Hyo-Jeong Kuh[a]

We have evaluated the antitumor effects of gefitinib (Iressa, ZD1839) in SNU-1 human gastric cancer cells (hMLH1-deficient and epidermal growth factor receptor-overexpressed) when given alone or as a doublet with oxaliplatin (LOHP), 5-fluorouracil (5-FU) or paclitaxel (PTX). The four drugs showed IC_{50}s ranging from 1.81 nM to 13.2 μM. LOHP and PTX induced G_2/M arrest, 5-FU increased S phase, and gefitinib increased G_1 in a concentration-dependent manner. The analysis using the previously developed cytostatic TP_I model showed that 64 and 80% of the overall growth inhibition was attributed to cell cycle arrest in cells exposed to 7.55 μM of LOHP or 10 nM of PTX for 72 h, respectively. PTX + gefitinib showed greatest synergism as determined by combination index analysis and apoptosis induced by PTX was potentiated by the co-administration of gefitinib. LOHP + gefitinib showed a similar, although to a lesser degree, synergistic effect. This study demonstrates the antitumor activity and the significant cell cycle arrest induced by gefitinib in SNU-1 human gastric carcinoma cells, and its synergistic interaction with LOHP and PTX. *Anti-Cancer Drugs* **15:809–818 © 2004 Lippincott Williams & Wilkins.**

Anti-Cancer Drugs 2004, 15:809–818

Keywords: combination, gefitinib (ZD1839), human gastric carcinoma, oxaliplatin, paclitaxel

[a]Research Institute of New Drug Development, Catholic Research Institutes of Medical Science and [b]Division of Medical Oncology, The Catholic University of Korea, Seoul, South Korea and [c]Support Facility of Project Ward, National Cancer Center Hospital, Tokyo, Japan

Sponsorship: This work was supported in part by a grant from the Korea Health 21 R&D Project, Ministry of Health & Welfare (02-PJ2-PG1-CH12-0002), and by a grant from KOSEF (R04-2000-000-00052-0), Republic of Korea.

Correspondence to H.-J. Kuh, Catholic Research Institutes of Medical Science, Catholic University of Korea, 505 Banpo-dong, Seocho-ku, Seoul 137-401, South Korea.
Tel: +82 2 590 2422; fax: +82 2 592 2421;
e-mail: hkuh@catholic.ac.kr

Received 23 February 2004 Revised form accepted 4 June 2004

Introduction

The contemporary combination regimens for treatment of gastric cancer usually contain cisplatin and 5-fluorouracil (5-FU). Recently, the triplet combination of cisplatin, 5-FU and paclitaxel (PTX) has become one of the most highly active regimens against advanced gastric carcinoma [1].

Tumor tissues from gastric cancer patients show a high incidence of epidermal growth factor (EGF) and its receptor (EGFR) overexpression, both of which play a promotional role in the development of gastric cancer cooperatively with other members of the EGFR gene family, c-erbB-2 and c-erbB-3 [2]. The EGF and EGFR gene families have been associated with the growth regulation and gastric wall invasion in gastric cancers [3,4], and seem to be involved in determining the chemosensitivity of human cancer cells to chemotherapy [5]. Recently, it was also reported that inhibition of the EGFR cascade abrogated *Helicobacter pyroli*-induced up-regulation of vascular endothelial growth factor in gastric cancer cells [6]. A novel approach for the therapeutic blockade of EGFR signaling in human cancer has been recently developed based on the discovery of low-molecular-weight compounds that selectively inhibit the ligand-induced activation of EGFR tyrosine kinase (TK) and its receptor-mediated intracellular signaling [7]. Among various quinazoline-derived compounds tested as new anticancer drugs, gefitinib ([4-(3-chloro-4-fluoro-anilino)-7-methoxy-6-(3-morpholinopropoxy) quinazoline], also 'Iressa', ZD1839) has shown impressive preclinical activity in various tumor models *in vitro* and *in vivo* [7]. It is an orally active, selective EGFR-TK inhibitor that blocks the signal transduction pathways implicated in the proliferation and survival of cancer cells, and is currently under phase III clinical trial [7,8].

In addition, the methylation of DNA mismatch repair (MMR) genes has been observed in many human cancers, including gastric cancers. The methylation of the hMLH-1 promoter region has been shown to be involved in the mechanism of low or undetectable hMLH-1 protein expression in gastric tumors [9,10]. In addition to predisposing oncogenesis, the loss of MMR activity is related to drug resistance, since the MMR proteins play important roles in mediating the activation of cell cycle checkpoints and apoptosis in response to DNA damage induced by anticancer agents. This drug resistance extends to a variety of alkylating anticancer agents including platinum compounds, such as cisplatin and carboplatin [11]. Moreover, it has been shown that *N*-methyl-*N'*-nitro-*N*-nitrosoguanidine (MNNG)-resistant

0959-4973

human gastric cancer cells have very low or undetectable levels of hMLH-1 protein, which plays a key role with hMSH2 in the MMR system [12].

Oxaliplatin (LOHP) has a spectrum of activity that differs from that of cisplatin or carboplatin, suggesting that it has different molecular targets and/or different mechanism of resistance. It has been reported that MMR deficiencies do not induce similar resistance to LOHP [13], and because of this decreased possibility of resistance development, LOHP may serve as a good candidate for first-line treatment as a monotherapy or in combination with other agents in gastric cancer. Hence, LOHP may effectively substitute for cisplatin in the platinum-based triplet combination with 5-FU and PTX, as mentioned above.

In many studies, gefitinib in combination with radiation as well as a variety of cytotoxic agents, including taxanes and platinum compounds, has shown synergistic and supra-additive interactions in many types of cancers, such as colon, lung, breast, prostate and ovarian cancer [14]. However, no studies have been conducted on the antitumor effects of gefitinib given alone or in combination with cytotoxic agents against human gastric cancer cells.

In the present study, we evaluated the growth-inhibitory and cell cycle arrest effects of LOHP, 5-FU and PTX, which are promising cytotoxic drugs for the treatment of gastric carcinoma, and of a target-based cytostatic drug, gefitinib, in SNU-1 human gastric carcinoma cells that show MMR deficiency and EGFR overexpression. We also determined whether simultaneous EGFR blockade by gefitinib could improve the anticancer activities of these cytotoxic drugs. Our results show that the gefitinib + PTX combination had the greatest synergistic interaction. Gefitinib was found to potentiate the apoptosis induced by PTX.

Materials and methods

Chemicals

Clinical grade gefitinib and LOHP were kindly provided by AstraZeneca Pharmaceuticals (Macclesfield, UK) and Sanofi-Synthelabo (Malvern, PA), respectively. PTX and 5-FU were provided by the Drug Synthesis and Chemistry Branch, Developmental Therapeutics Program, Division of Cancer Treatment and Diagnosis, NCI (Bethesda, MD). Other drugs and reagents, unless otherwise stated, were purchased from Sigma (St Louis, MO).

Cell culture conditions

The human gastric cancer cell lines, SNU-1 and MKN-45, human lung adenocarcinoma cell line, A549, and human epidermoid carcinoma cell line, A431 were obtained from the Korean Cell Line Bank (Seoul, South Korea). Cells were maintained in RPMI 1640 supplemented with 10% heat-inactivated fetal bovine serum, 100 mg/ml of streptomycin and 100 U/ml penicillin in humidified air containing 5% (v/v) CO_2 at 37°C.

Western blotting

Total cell protein extracts were obtained as previously described [15]. Briefly, cells were lysed with lysis buffer [20 mM Tris–HCl (pH 7.5), 150 mM NaCl, 0.1% SDS, 1% Triton X-100, 1% sodium deoxycholate]. The lysate, containing 30 μg of total protein, was then mixed with 2 × SDS–PAGE sample buffer, boiled for 5 min and electrophoresed in 8% SDS gels under reducing conditions. The separated proteins were then electrophoretically transferred to PVDF membranes (Millipore, Bedford, MA) and the membranes were probed with a primary antibody against EGFR or hMLH1 (anti-human EGFR rabbit polyclonal antibody and anti-human hMLH1 rabbit polyclonal antibody; Santa Cruz Biotechnology, Santa Cruz, CA) at 1:1000 dilution. Immunoreactive proteins were detected by using an enhanced chemiluminescence detection system (Amersham Pharmacia Biotech, Little Chalfont, UK).

Measurement of growth inhibition

Growth inhibitory effects were measured by MTT assay and by direct cell counting [16]. For MTT assay, cells were plated in 96-well microtiter 24 h prior to treatment (4000 cells/well). Cells were exposed to various concentrations of the tested agents for 72 h. The absorbance of the reaction mixture was measured at 540 nm and the IC_{50} defined as the drug concentration required to reduce the absorbance to 50% of the control in each test was determined using an E_{max} model:

$$\%\ \text{Cell viability} = (100 - R) \times \left(1 - \frac{[D]^m}{K_d^m + [D]^m}\right) + R \quad (1)$$

where D is the drug concentration, K_d is the concentration of the drug that produces a 50% reduction in absorbance (i.e. IC_{50}), m is the Hill-type coefficient and R is the residual unaffected fraction (the resistant fraction). The Sigma Plot regression function was used for model fitting.

For direct cell counting, cells were seeded at a density of 1×10^6 in 100- or 150-mm Petri dishes at least 24 h prior to drug exposure and were exposed to two different concentrations of the drug for up to 72 h. The concentrations of each drug were 0.75 and 7.55 μM for LOHP, 9 and 65 μM for 5-FU, 2.5 and 10 nM for PTX, and 13 and 38 μM for gefitinib. At predetermined times, cells were harvested by resuspending then in PBS and then the total cell number was determined using a Counter (Coulter Electronics, Luton, UK). Trypan blue

exclusion under the microscope was used to determine the viable cell fraction. The remainder of the cell suspension samples was used for the cell cycle study (see below). For the combination study, gefitinib was given simultaneously with either LOHP, 5-FU or PTX for 72 h. Drugs were combined at equitoxic ratios (i.e. doses were applied in combinations that would have produced the same cytotoxic effect if the drugs were administered separately to produce a 50% growth inhibition, as determined by MTT assay). The cytotoxicities of the two-drug combinations were determined by MTT assay using the same procedure as used for single treatments. Each experiment was performed in triplicate.

Determination of combination effects

The cytotoxic effects obtained with two-drug combinations were analyzed using the Chou and Talalay method [17]. The interaction between two drugs was assessed by using combination index (CI) (2). CI was calculated for a cell death range of 20–80 %, i.e. CI_{20}–CI_{80}.

$$CI_x = \frac{(D)_A}{(D_x)_A} + \frac{(D)_B}{(D_x)_B} + \alpha \cdot \frac{(D)_A(D)_B}{(D_x)_A(D_x)_B} \qquad (2)$$

where CI_x is the CI for a fixed effect, x [fraction affected $(f_a)\cdot 100$], for a combination of drug A and drug B, $(D_x)_A$ is the concentration of drug A alone giving an effect x, $(D_x)_B$ is the concentration of drug B alone giving an effect x, $(D)_A$ is the concentration of drug A in combination A + B giving an effect x, $(D)_B$ is the concentration of drug B in combination A + B giving an effect x, and α is a parameter with value 0 when A and B are mutually exclusive and 1 when A and B are mutually non-exclusive. A CI_x between 0.8 and 1.2 was categorized as additive, less than 0.8 as synergistic, and greater than 1.2 as antagonistic.

Measurement of cell cycle effect

Cells were plated and treated as described above (see measurement of growth inhibition by direct cell counting). For the combination of PTX and gefitinib, cells were exposed to 1.25 nM of PTX and 8.5 μM of gefitinib or 0.6 nM of PTX and 4 μM of gefitinib. After harvesting, the cells were fixed in 10 ml of 70% cold ethanol while vortexing, and cells were kept at 4°C for 1 h and stored at −20°C until analysis. Upon analysis, fixed cells were washed and resuspended in 1 ml of PBS containing 50 μg/ml RNase A and 50 μg/ml propidium iodide. After 20 min incubation at 37°C, cells were analyzed for DNA content by flow cytometry (FACSVantage; Becton Dickinson Immunocytometry Systems, San Jose, CA). For each sample, 10 000 events were acquired. Cell cycle distribution was determined using cell cycle analysis software (Modfit; Verity, Topsham, ME).

Cytostatic model analysis

In order to predict the contribution of cell cycle arrest to the overall growth inhibition induced by a cytotoxic agent, we used the cytostatic TP_i model as described previously [18]. In brief, the model assumptions were: (1) exponential growth of a cell population with a growth rate constant (k); (2) all cells were in cycle, i.e. no cell deaths and no G_0 phase arrest; (3) that the distribution of cell numbers in a cell cycle follows the age structure of a simple exponential population. $TP_i(t)$, the transition probability for i phase at time t, was defined as $(\alpha_i(t)-\alpha_i(t+\Delta t))/\alpha_i(t)/\Delta t$, where $\alpha_i(t) = [N_i(t)-(\#$ cells already exiting from i phase at time $t)]/N_i(t)$ and $N_i(t)$ is the number of cells in i phase at time t. The transition probability for each cell cycle check point, i.e. $TP_{G1}(t)$, $TP_S(t)$ and $TP_{G2/M}(t)$, was calculated using $F_i(t)$, the fraction of cells in the G_1, S and G_2/M phases at time t, and $k(t)$, the growth rate constant. The simulation of cell population growth over time was performed using a numerical method based on the cell population growth algorithm using $TP_i(t)$ and $F_i(t)$. This model assumes no cell death during cell cycle progression; hence, the simulation result represents a reduction in the number of cells resulting from cell cycle arrest (or disturbed cell cycle progression) only. The model should underestimate growth inhibition in the presence of cell death and the difference between the model-predicted and the observed growth curve of a treated cell population represents the growth inhibition resulting from cell death in the population.

Simultaneous measurement of drug-induced apoptosis and cell cycle distribution

For simultaneous determination of cell cycle contents and apoptosis, the user's manual of Apo-Direct kit (PharMingen, San Diego, CA) was followed. Briefly, after harvest, cells were fixed in 1% paraformaldehyde/PBS on ice for 15 min and resuspended in 70% ice-cold ethanol. Cells were then incubated in 50 μg of solution containing terminal deoxynucleotidyltransferase and FITC-conjugated dUTP deoxynucleotides 1:1 in reaction buffer for 2 h at 37°C in the dark. After washing in PBS containing 0.1% Triton X-100, the cells were stained with 5 μg of propidium iodide and 10 kU of RNase in 1 ml of PBS for 20 min at 37°C. Flow cytometric analysis was performed with FL1 (FITC) and FL2 (propidium iodide) and data acquisition and analysis were done using CellQuest software (Becton Dickinson Immunocytometry Systems).

Statistical analysis

Statistical comparisons were completed using Student's paired t-test; $p < 0.05$ was considered statistically significant.

Results

hMLH-1 and EGFR expression in SNU-1 and MKN45

We evaluated the antitumor activities of the three cytotoxic drugs, LOHP, 5-FU or PTX, and that of a cytostatic drug, gefitinib, alone and in doublet combinations. We selected SNU-1 human gastric carcinoma cells because they are known to be MMR deficient due to a

missense mutation in hMLH-1 [12], which was confirmed in this study (Fig. 1A). EGFR expression was also examined and significant expression was observed in these cells. The level of expression was higher than those in MKN-45, another human gastric cancer cell line, and in A549, a human lung cancer cell line (Fig. 1B and 1C). Hence, SNU-1 cells were considered to represent an *in vitro* gastric cancer model that may have intrinsic chemoresistance related to both MMR deficiency and EGFR overexpression.

Cytotoxicity of LOHP, 5-FU, PTX and gefitinib in SNU-1 cells

Dose–response curves were analyzed using an E_{max} model with a resistant fraction (R), which represents the fraction of cells insensitive to the drug (Table 1). Significant R values were obtained for PTX (mean of 32%), whereas the other three drugs showed a full dose–response curve with percentage cell viabilities decreasing almost to the base line level (< 10%). The IC_{50} showed a wide range from 1.81 nM to 13.2 μM, i.e. 0.788 μM for LOHP, 9.35 μM for 5-FU, 1.81 nM for PTX and 13.2 μM for gefitinib. The antiproliferative activity of these agents was confirmed by direct cell counting. Drugs were given at two different concentrations, i.e. at the IC_{50} and IC_{80} levels. For all agents, 72 h exposure exhibited 50–60 and 80–90% growth inhibition at the IC_{50} and IC_{80} drug concentrations, respectively (Fig. 2). For PTX, 10 nM induced 68% growth inhibition when measured by MTT assay, with no further inhibition at higher concentrations, nonetheless, 89% inhibition was observed by direct cell counting (Fig. 2C).

Fig. 1

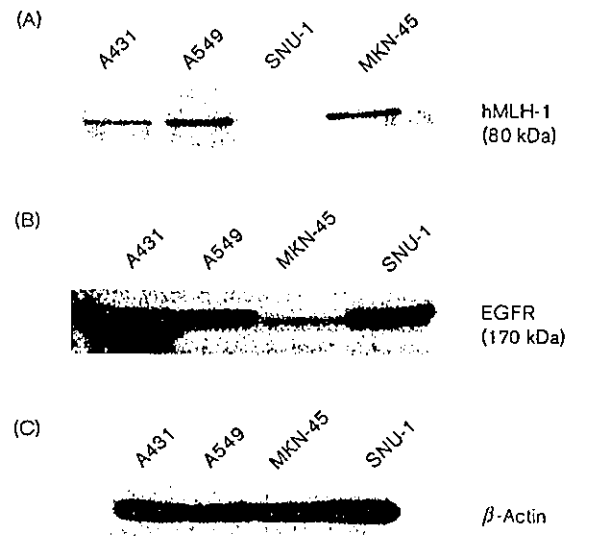

Western blot analysis of hMLH-1 (A) and EGFR (B) expression in A549, A431, SNU-1 and MKN-45 cells. The relative expression levels of EGFR relative to β-actin (C) were compared for these four cell lines.

Cytostatic model analysis

Growth inhibition, i.e. the reduction in the growth rate of a cell population following drug treatment, is the result of cell cycle arrest (cytostatic effect) and cell death (cytotoxic effect). As previously reported, we have developed a computational model (a cytostatic model, because the model assumes no cell death to predict the growth inhibition resulting from cell cycle arrest only) to assess the respective contributions of cell cycle arrest and cell death to the overall growth inhibition induced by cytotoxic anticancer agents [18]. We used this cytostatic model to analyze the contribution of cell cycle arrest to overall growth inhibition when SNU-1 cells were treated with each cytotoxic agent. The time course of cell cycle distribution was determined in SNU-1 cells exposed to LOHP, 5-FU and PTX at IC_{80} levels, respectively, and used in model simulation (part of data shown in Fig. 3). Since the model uses the percentage of cells in each phase to simulate the growth of a cell population, predictions cannot be made with 0% in any phase at anytime. For this reason, this cytostatic model was used only for LOHP and PTX, but not for 5-FU, because in this case the percentage of cells in the G_2/M phase was zero after 12 h exposure (data not shown). The cytostatic computational model predicted 64% of the overall inhibition from the cell cycle arrest induced by LOHP after 72 h exposure at 7.55 μM. For PTX given for 72 h at 10 nM and 80% of the overall inhibition was attributed to cell cycle arrest by the model. These results indicate that the reduction in population growth rate caused by cell

Table 1 Parameters of the antiproliferative activities of LOHP, 5-FU, PTX and gefitinib against SNU-1 human gastric carcinoma cells

	LOHP	5-FU	PTX	Gefitinib
IC_{50}[a]	0.788 ± 0.142	9.35 ± 1.57	1.81 ± 0.67	13.2 ± 0.33
R[b]	5.00 ± 4.48	8.53 ± 7.64	32.0 ± 11.1	0
m[c]	0.811 ± 0.135	0.793 ± 0.125	5.02 ± 0.80	1.14 ± 0.10

Each value represents mean ± SD of three independent experiments.
[a]IC_{50} is the concentration of the drug that kills 50% of cancer cells compared to the control after 72 h of continuous exposure. Expressed in μM, except for paclitaxel, which is in nM.
[b]R is the residual unaffected fraction (resistance fraction) (1) and is equal to (100 − E_{max}).
[c]m is the Hill-type coefficient (1).

Fig. 2

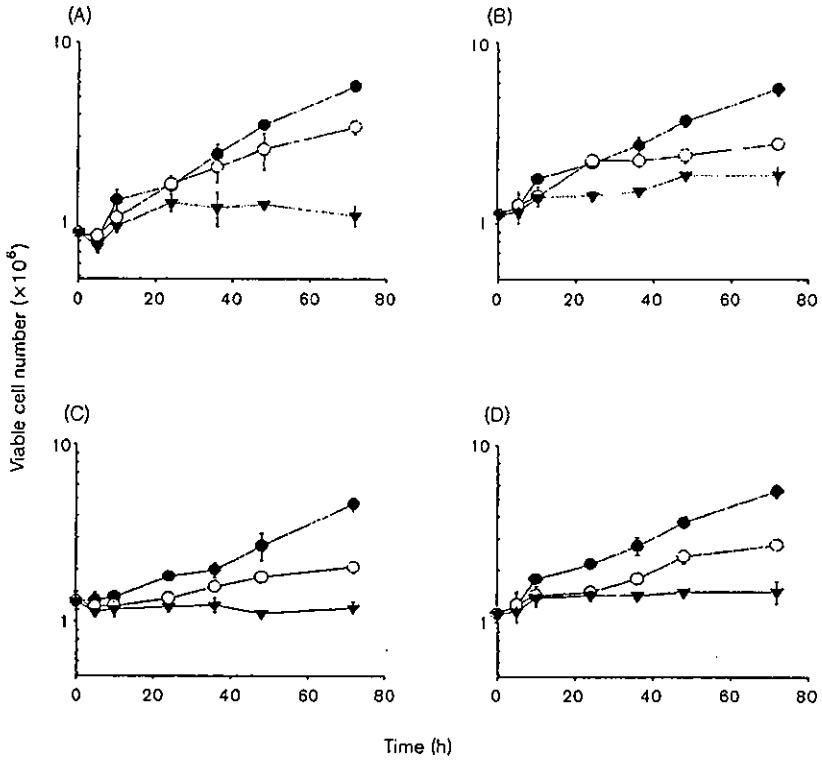

Growth curves of SNU-1 cells when incubated with (open circles, solid triangles) and without (solid circles) drug treatment: LOHP (A), 5-FU (B), PTX (C) and gefitinib (D). Cells were treated at two different concentrations near the IC_{50} (open circles) and the IC_{80} (solid triangles). The concentrations were: 0.75 and 7.55 μM for LOHP, 9 and 65 μM for 5-FU, 2.5 and 10 nM for PTX, and 13 and 38 μM for gefitinib. For cell number counting, cells were harvested by resuspending in medium and counted using a Coulter counter. Trypan blue exclusion was used for the determination of viable cell fraction.

cycle arrest effects contributes significantly to the overall growth inhibition induced by LOHP and PTX.

Cell cycle arrest effect with single drug treatment

The cell cycle arrest effect of the four agents was studied following a single drug exposure at two different concentrations for 72 h, i.e. around IC_{50} and IC_{80} as determined from the MTT dose–response curves. For LOHP, exposure to IC_{50} level concentrations, 0.75 μM did not induce significant changes in the cell cycle distribution (Fig. 3). When exposed to IC_{80} level concentrations, 7.55 μM of LOHP showed a moderate S phase decrease and G_2/M phase increase. Exposure to 5-FU (9 and 65 μM) resulted in an S phase increase along with G_2/M phase decreases in a concentration dependent manner: the cell cycle change following 5-FU treatment at the higher concentration (IC_{80}) was more pronounced. For LOHP and 5-FU, the sub-G_1 population, representative of cells that had undergone apoptosis, increased with time- and concentration-dependent manner. For PTX, cell cycle effect was dependent on drug concentration. At IC_{50} (2.5 nM), the number of cells in G_1 phase decreased with rapid accumulation of cells in sub-G_1 phase. At 10 nM, however, most cells were blocked in G_2/M phase (69.5 ± 0.8%) and a parallel decrease of the G_1 population was observed at 24 h, and a significant increase of the sub-G_1 population (27.4 ± 0.4%) and polyploid cells with ≥ 4*n* at 72 h. Gefitinib (13 and 38 μM) also showed a concentration dependent pattern of G_1 phase cell cycle arrest. The sub-G_1 population was induced after 72 h exposure at IC_{50} concentration (12.5 ± 1.6%) and increased to 52% after 72 h exposure at the concentration of 38 μM.

Evaluation of synergism

We evaluated the synergistic interaction between the cytotoxic agents, LOHP, 5-FU or PTX, and the cytostatic agent, gefitinib. All combinations were given at equitoxic ratios at the 50% inhibition levels of each drug, i.e. IC_{50} of drug A:IC_{50} of drug B. The dose–response curves are shown in Fig. 4 and the CI_x values calculated for $0.2 \leq f_a \leq 0.8$ (i.e. $20 \leq x \leq 80$) are shown in Fig. 5. CI_x values for the combination LOHP + gefitinib varied with f_a: CI_x decreased from 1.74 at $f_a = 0.2$ to 0.67 at $f_a = 0.8$. In the clinically relevant range of $f_a \geq 0.5$, hence, LOHP + gefitinib was considered to be synergistic to

Fig. 3

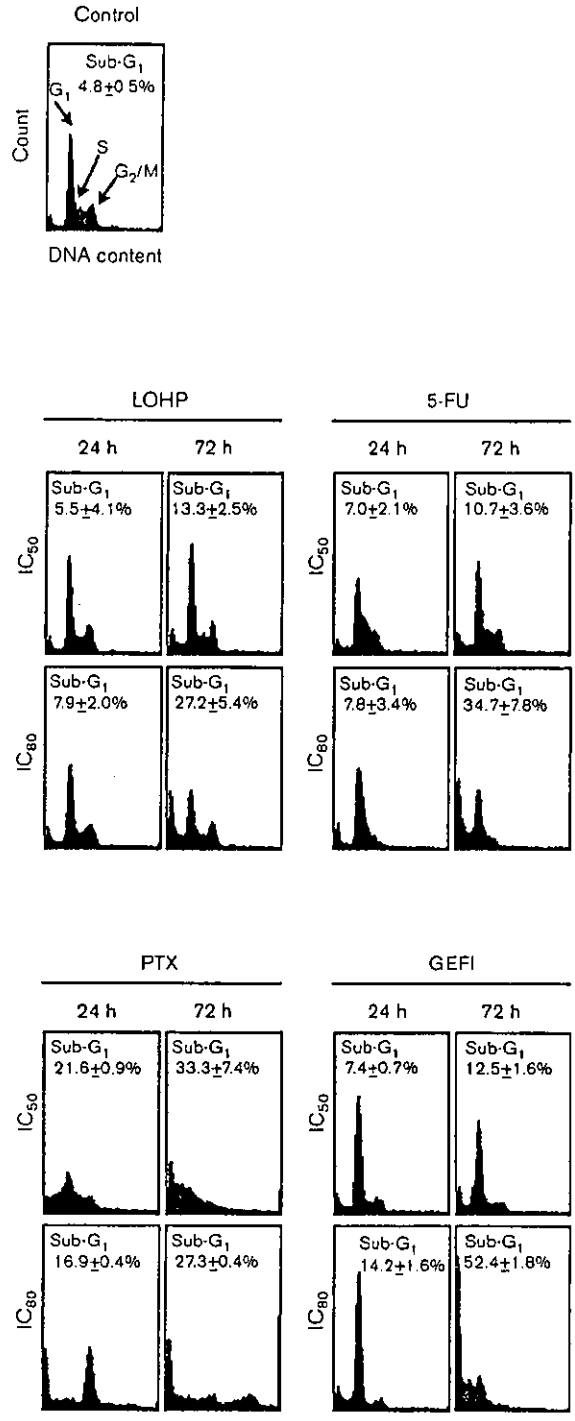

DNA histogram analysis in cells exposed to LOHP, 5-FU, PTX and gefitinib (GEFI) single treatment at IC_{50} and IC_{80}. Representative histograms are shown for 24 and 72 h post-treatment with the percentage of cells in sub-G_1 phase. Cells were harvested and fixed with ethanol before treated with RNase. Cells were then stained with propidium iodide and analyzed by flow cytometry. The concentrations were: 0.75 and 7.55 μM for LOHP, 9 and 65 μM for 5-FU, 2.5 and 10 nM for PTX, and 13 and 38 μM for GEFI.

additive. 5-FU + gefitinib was found additive with CI values ranging from 1.06 to 1.24. The combination of PTX + gefitinib showed greatest synergism: with CI values of less than 1.0 (0.28–0.99) for the whole f_a range; in particular, the resistant fraction associated with PTX single treatment was abrogated when combined with gefitinib, indicating a greater advantage compared to the other combinations (Fig. 4). For PTX + gefitinib, the most synergistic combination, the cell cycle arrest and apoptosis induction were studied in cells exposed to the simultaneous treatment of PTX and gefitinib at two different concentrations, i.e. 0.62 nM PTX + 4 μM gefitinib (combination IC_{50}) and 1.25 nM PTX + 8.5 μM gefitinib (combination IC_{65}) (Fig. 6). No significant changes in the cell cycle distribution were observed at the combination IC_{50} level until 72 h. At the higher concentration, i.e. 1.25 nM PTX + 8.5 μM gefitinib (around IC_{65}), a significant decrease in G_1 phase cells occurred with rapid increase in sub-G_1 cells. The simultaneous staining of DNA content and DNA strand breaks were used to discern the apoptotic cells as well as necrotic cells from viable cells (Fig. 6). The combination of PTX and gefitinib at the IC_{50} and IC_{65} level induced 100 and 35% increase ($p < 0.05$) in apoptosis (TUNEL-positive cells), respectively, compared to the single treatment, supporting the synergism between these two drugs.

Discussion

Systemic chemotherapy for the treatment of gastric carcinomas includes mitomycin C, anthracyclines, alkylating agents and 5-FU. Among these drugs, cisplatin and 5-FU are most commonly used in combination regimens. Recently, PTX has been added and a triplet combination of PTX, 5-FU and cisplatin has also been evaluated for the treatment of advanced gastric cancer [20]. In addition, a new platinum compound, LOHP, may replace cisplatin due to its reduced toxicity and decreased possibility of resistance development related to MMR deficiency. Hence, we undertook to evaluate in human gastric cancer cells the antitumor activities of LOHP, 5-FU and PTX, and the potential synergistic interactions between these cytotoxic agents individually and a newly developed target-based (cytostatic) drug, gefitinib, to provide preclinical data for the future clinical development of these agents in a combination setting for the treatment of advanced gastric carcinomas.

The *in vitro* antitumor activity of the four agents was evaluated by MTT assay. SNU-1 cells showed differential sensitivity toward these agents, and the rank order of sensitivities was PTX (1.81 nM) > LOHP (0.788 μM) > 5-FU (9.35 μM) > gefitinib (13.2 μM). Among these four agents, PTX showed the greatest cytotoxicity with an IC_{50} in the nanomolar range; however a significant

Fig. 4

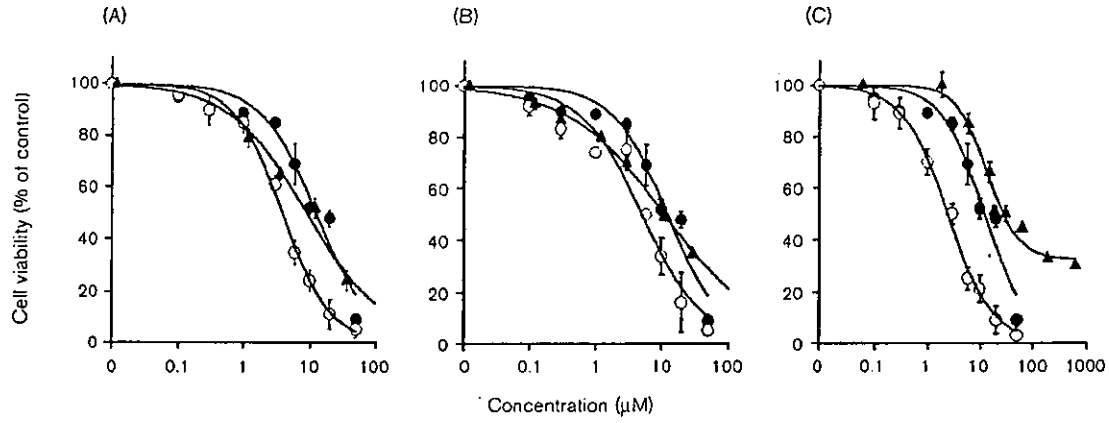

Representative dose–response curves of LOHP, 5-FU, PTX and gefitinib administered alone and in combination. (A) Gefitinib alone (solid circles), LOHP alone (solid triangles), LOHP + gefitinib (open circles); (B) gefitinib alone (solid circles), 5-FU alone (solid triangles), 5-FU + gefitinib (open circles); and (C) gefitinib alone (solid circles), PTX alone (solid triangles), PTX + gefitinib (open circles). Cells were simultaneously exposed to each treatment regimen for 72 h and cell viability was determined by MTT assay. The *x*-axis is [gefitinib] × 1, [LOHP] × 12, [5-FU] × 1.2 and [PTX] × 6250.

fraction of resistant cells was found (Table 1). Such PTX-resistant fractions have been observed in other cell lines, such as A549, a human lung adenocarcinoma cell line, and in FaDu, a pharynx squamous carcinoma cell line, when cell viability was measured by the MTT or the SRB assay (unpublished data). In the case of PTX, the growth-inhibitory effect as measured by two different methods produced different results, i.e. MTT versus direct cell counting (Table 1 and Fig. 2). The exposure of cells to 10 nM of PTX for 72 h induced around 90% growth inhibition, when determined by direct cell counting, whereas 68% growth inhibition was expected based on MTT data. In the cases of the other three agents, the MTT data agreed with direct cell counting. Therefore, the resistant fraction obtained in the MTT assay seemed to be associated with the assay method, especially for PTX, suggesting that the experimental data obtained by widely used viability assays, such as MTT and SRB, should be interpreted with caution when determining the cytotoxicity of PTX in monolayer cultures. However, in the present study, this did not affect the degree of synergy calculated for gefitinib + PTX since the maximum concentration of PTX used for the CI calculation was 2.5 nM, where no difference was observed between the cell counting and MTT results (Fig. 2).

Fig. 5

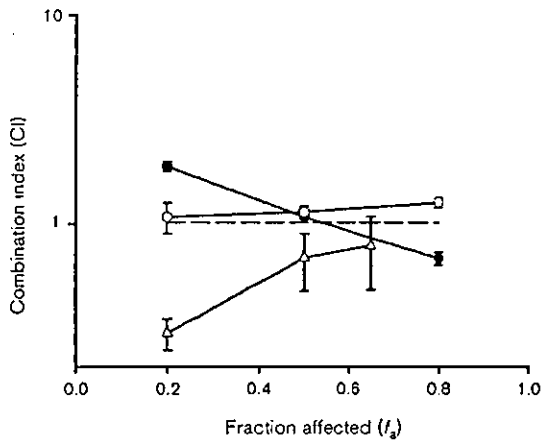

Combination index (CI_x) versus affected fraction (f_a) plots for LOHP + gefitinib (solid circles), 5-FU + gefitinib (open circles) and PTX + gefitinib (open squares) in SNU-1 cells. Cells were treated with LOHP or 5-FU or PTX + gefitinib at fixed equitoxic ratios. CI < 0.8, CI = 1 and CI > 1.2 indicate synergism, additivity and antagonism, respectively. LOHP and gefitinib were treated at a 0.083:1 molar ratio, 5-FU and gefitinib at 0.83:1, and PTX and gefitinib at 0.00016:1. CI_x was calculated using E_{max} model parameters obtained from the MTT data shown in Fig. 4.

SNU-1 cells showed significant resistance to 5-FU, i.e. the IC_{50} of 5-FU in SNU-1 cells was rather high (9.35 μM), which is close to that of gefitinib, a known cytostatic drug. MMR-proficient MKN-45 cells showed about 3 times higher sensitivity to 5-FU than SNU-1 cells (unpublished data). Hence, this intrinsic resistance of SNU-1 to 5-FU may be related to its MMR deficiency [15].

It has been suggested that the inhibition of EGFR-TK is an effective antiproliferative principle in EGFR-positive human gastric cancer cells [4]. Recently, gefitinib showed antiangiogenic and antiproliferative activity in a variety of human cancer cells *in vitro*, including human gastric cancer cells (KATO III and N87) [21]. The cytostatic growth inhibitory activity of gefitinib has been

Fig. 6

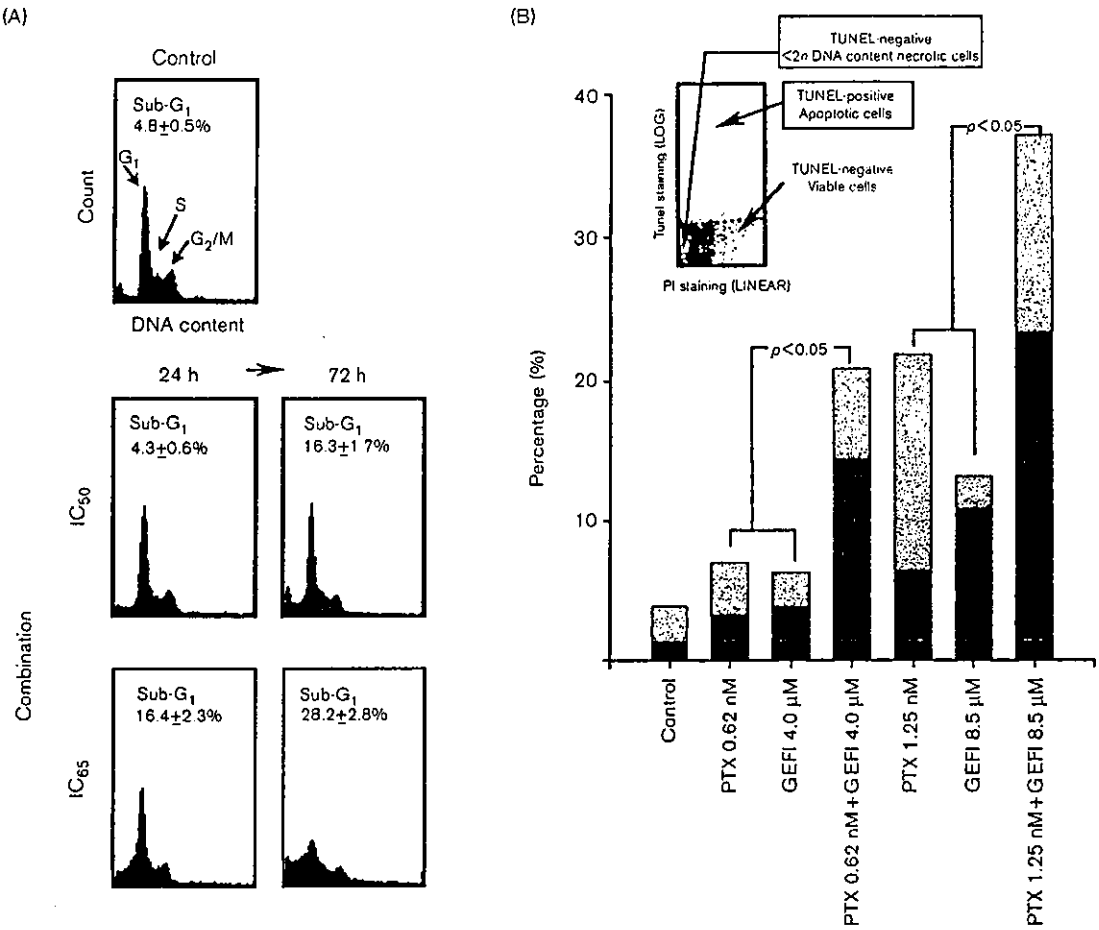

Cell cycle distribution and apoptosis induction during simultaneous treatment with PTX and gefitinib in SNU-1 cells. The drug concentrations used were 0.6 nM PTX + 4 μM (IC_{50}) or 1.25 nM PTX + 8.5 μM gefitinib (IC_{65}). (A) Representative histograms are shown for 24 and 72 h post-treatment with the percentage of cells in the sub-G_1 phase. At predetermined times following drug exposure, cells were harvested, fixed, stained with propidium iodide (PI) and analyzed by flow cytometry. (B) The bivariate analysis of DNA content and apoptosis in cells exposed to the indicated drug treatment for 72 h. Cells were treated for 72 h and processed for the double staining of TUNEL/PI and analyzed by flow cytometry. Solid box: TUNEL-negative necrotic cells; gray box: TUNEL-positive apoptotic cells. Statistical analysis: sum of PTX and gefitinib alone versus combination: $p<0.05$.

demonstrated in a wide range of human cancer cell lines, and the reported IC_{50}s of gefitinib vary by cell line and by the assay method used. A soft agar colony assay showed an IC_{50} range of 0.05–2.5 μM for gefitinib in breast, colon and gastric cancer cells [8,21]. On the other hand, an IC_{50} range of 6–30 μM was reported in human head/neck and colon cancer cells by MTT [22,23]. Our results on the antitumor activity of gefitinib in SNU-1 cells are comparable with those obtained using the same viability assay method, i.e. MTT (Table 1).

A few studies have demonstrated an inverse correlation between growth IC_{50} and EGFR expression level [22], whereas contradictory data have been reported by others [7]. SNU-1 cells express moderate levels of EGFR, which may explain its moderate IC_{50} compared to other studies, which used highly overexpressing cell lines, such as A431. The EGFR signaling pathway involves the activation of several nuclear proteins, including cyclin D_1, via the activation of *ras* and mitogen-activated protein kinase [21]. Since EGFR activates cyclin D_1, and cyclin D_1 is required for cell cycle progression from G_1 to the S phase, EGFR signaling is critical for cell proliferation and its inhibition causes G_1 arrest in human cancer cells [21]. Our results also demonstrate that the inhibition of EGFR signaling by gefitinib induces G_1 arrest in human gastric cancer cells in a concentration dependent manner (Fig. 3).

In common with other cytostatic agents, gefitinib is expected to be a good candidate for combination regimens with cytotoxic agents. The combination of gefitinib + PTX has been shown to induce dose-depen-

dent cooperative growth inhibition and the potentiation of apoptosis *in vitro* [8,21], and to induce complete regression in some human tumor xenograft models [7]. Gefitinib + LOHP has been found to be supra-additive in human ovarian, breast and colon cells [14,24]. The sequence-dependent synergy appeared to be cell-line specific, i.e. gefitinib followed by cisplatin/5-FU was synergistic in head/neck cell cancer cell line [22], whereas gefitinib followed by oxaliplatin was antagonistic in human colon cancer cell line [25]. The simultaneous exposure was additive to synergistic in both studies, hence, the simultaneous schedule was to chosen to evaluate the synergy in the present study. We did not evaluate the sequence-dependent interactions because SNU-1 cells grow as a suspension and, hence, are not suitable for such experiments. The sequence dependency should be investigated using another human gastric cancer cell line.

In the present study, CI_x was calculated for the range of $0.2 \leq f_a \leq 0.8$ (Fig. 5), but the combination effect on cell cycle distribution and apoptosis induction was evaluated for the range of $f_a \geq 0.5$, i.e. at IC_{50} and IC_{80} levels (Fig. 6). Considering the fact that the maximum effect is needed in the clinical situation, it should be more relevant to focus on the effect above IC_{50} level [22]. Preclinical studies (especially, animal models) commonly use lower doses of chemotherapy to observe greater synergy; however, this often do not translate to the clinic, where maximum therapeutic doses are used [26].

In our study, the potentiation of antitumor activity was greatest for PTX + gefitinib, which had the lowest CI_{50} value among the three combinations and moreover the resistant fraction in the PTX single treatment was completely abrogated (Figs 4 and 5). LOHP + gefitinib is also a promising combination regimen because it produced a very similar level of synergism to PTX + gefitinib at $f_a = 0.8$ and additive effects at the $f_a = 0.5$ level. Gefitinib combined with PTX resulted in enhanced drug-induced apoptosis (Fig. 6). It is conceivable that the cytotoxicity of PTX is potentiated by the effective inhibition of survival signals upregulated by the EGFR signal network. The elucidation of the mechanism of this interaction requires further investigation.

Results of phase III lung trials for gefitinib + cytotoxics were disappointing and can be attributed to many factors including the following: (i) due to the lack of correlation between the apparent expression of EGFR and sensitivity, the responding phenotype was not known and patient selection could not be made, (ii) it is believed that triplet regimen of conventional chemotherapy are not superior to doublets in non-small cell lung cancer, and (iii) patients (in IDEAL phase II trials) who were already heavily treated with, and refractory to, chemotherapy may have been more sensitive to the inhibition of the EGFR pathway by gefitinib [27]. Despite the negative results of phase III lung trials, the rationales for studying the combination of gefitinib with cytotoxics in gastric cancers are 3-fold. (i) EGFR levels were associated with poor prognosis in gastric cancer patients [28,29], (ii) gefitinib is given orally, hence, higher drug concentration can be obtained in the gastric tissues and (iii) gastric cancers are relatively easy for biopsy study through which the responding phenotype can be identified.

In summary, the present study demonstrates that the antitumor activity of gefitinib, against human gastric carcinoma cells, is accompanied by significant cell cycle arrest and apoptosis. We also found that the antiproliferative effects of the cytotoxic drugs, LOHP and PTX, could be greatly enhanced when combined with gefitinib. The suppression of growth by gefitinib may be of clinical importance as the prolonged administration of orally active gefitinib could offer long-term control of gastric tumor growth and metastasis. This study provides preclinical data supporting the clinical development of gefitinib and its use in combination with PTX or LOHP against MMR-deficient human gastric cancers that express EGFR. Moreover, this study shows that gefitinib warrants further evaluation *vis-à-vis* its use in other gastric cancer cells/tumors.

References

1 Kim YH, Shin SW, Kim BS, Kim JH, Kim JG, Mok YJ, *et al.* Paclitaxel, 5-FU, and cisplatin combination chemotherapy for the treatment of advanced gastric carcinoma. *Cancer* 1999; 85:295–301.

2 Slesak B, Harlozinska A, Porebska I, Bojarowski T, Lapinska J, Rzeszutko M, *et al.* Expression of epidermal growth factor receptor family proteins (EGFR, c-erbB-2 and c-erbB-3) in gastric cancer and chronic gastritis. *Anticancer Res* 1998; 18:2727–2732.

3 Aoyagi K, Kohfuji K, Yano S, Murakami N, Miyagi M, Takeda J, *et al.* Evaluation of the epidermal growth factor receptor (EGFR) and c-erbB-2 in superspreading-type and penetrating-type gastric carcinoma. *Kurume Med J* 2001; 48:197–200.

4 Piontek M, Hengels KJ, Porschen R, Strohmeyer G. Antiproliferative effect of tyrosine kinase inhibitors in epidermal growth factor-stimulated growth of human gastric cancer cells. *Anticancer Res* 1993; 13:2119–2123.

5 Mendelsohn J, Fan Z. Epidermal growth factor receptor family and chemosensitization. *J Natl Cancer Inst* 1997; 89:341–343.

6 Caputo R, Tuccillo C, Manzo BA, Zarrilli R, Tortora G, Blanco Cdel V, *et al.* *Helicobacter pylori* VacA toxin up-regulates vascular endothelial growth factor expression in MKN 28 gastric cells through an epidermal growth factor receptor-, cyclooxygenase-2-dependent mechanism. *Clin Cancer Res* 2003; 9:2015–2021.

7 Sirotnak FM, Zakowski MF, Miller VA, Scher HI, Kris MG. Efficacy of cytotoxic agents against human tumor xenografts is markedly enhanced by coadministration of ZD1839 (Iressa), an inhibitor of EGFR tyrosine kinase. *Clin Cancer Res* 2000; 6:4885–4892.

8 Ciardiello F, Caputo R, Borriello G, Del Bufalo D, Biroccio A, Zupi G, *et al.* ZD1839 (IRESSA), an EGFR-selective tyrosine kinase inhibitor, enhances taxane activity in *bcl*-2 overexpressing, multidrug-resistant MCF-7 ADR human breast cancer cells. *Int J Cancer* 2002; 98:463–469.

9 Bevilacqua RA, Simpson AJ. Methylation of the hMLH1 promoter but no hMLH1 mutations in sporadic gastric carcinomas with high-level microsatellite instability. *Int J Cancer* 2000; 87: 200–203.

10 Kang YH, Bae SI, Kim WH. Comprehensive analysis of promoter methylation and altered expression of hMLH1 in gastric cancer cell lines with microsatellite instability. *J Cancer Res Clin Oncol* 2002; 128:119–124.

11 Fink D, Aebi S, Howell SB. The role of DNA mismatch repair in drug resistance. *Clin Cancer Res* 1998; 4:1–6.

12 Shin KH, Yang YM, Park J-G. Absence or decreased levels of the hMLH-1 protein in human carcinoma cell lines: implication of hMLH-1 in alkylation tolerance. *J Cancer Res Clin Oncol* 1998; 124:421–426.
13 Raymond E, Faivre S, Woynarowski JM, Chaney SG. Oxaliplatin: mechanism of action and antineoplastic activity. *Semin Oncol* 1998; 25:4–12.
14 Ciardiello F, Caputo R, Bianco R, Damiano V, Pomatico G, De Placido S, *et al.* Antitumor effect and potentiation of cytotoxic drugs activity in human cancer cells by ZD-1839 (Iressa), an epidermal growth factor receptor-selective tyrosine kinase inhibitor. *Clin Cancer Res* 2000; 6:2053–2063.
15 Carethers JM, Chauhan DP, Fink D, Nebel S, Bresalier RS, Howell SB, *et al.* Mismatch repair proficiency and *in vitro* response to 5-fluorouracil. *Gastroenterology* 1999; 117:123–131.
16 Carmichael J, Mitchell JB, DeGraff WG, Gamson J, Gazdar AF, Johnson BE, *et al.* Chemosensitivity testing of human lung cancer cell lines using the MTT assay. *Br J Cancer* 1988; 57:540–547.
17 Chou TC, Talalay P. Quantitative analysis of dose-effect relationships: the combined effects of multiple drugs or enzyme inhibitors. *Adv Enz Reg* 1984; 22:27–55.
18 Kuh HJ, Nakagawa S, Usuda J, Yamaoka K, Saijo N, Nishio K. A computational model for quantitative analysis of cell cycle arrest and its contribution to overall growth inhibition by anticancer agents. *Jpn J Cancer Res* 2000; 91:1303–1313.
19 Steel GG. *Growth Kinetics of Tumors: Cell Population Kinetics in Relation to the Growth and Treatment of Cancer.* Oxford: Clarendon Press; 1977.
20 Honecker F, Kollmannsberger C, Quietzsch D, Haag C, Schroeder M, Spott C, *et al.* Phase II study of weekly paclitaxel plus 24-h continuous infusion 5-FU, folinic acid and 3-weekly cisplatin for the treatment of patients with advanced gastric cancer. *Anticancer Drugs* 2002; 13:497–503.
21 Ciardiello F, Caputo R, Bianco R, Damiano V, Fontanini G, Cuccato S, *et al.* Inhibition of growth factor production and angiogenesis in human cancer cells by ZD1839 (Iressa), a selective epidermal growth factor receptor tyrosine kinase inhibitor. *Clin Cancer Res* 2001; 7: 1459–1465.
22 Magne N, Fischel JL, Dubreuil A, Formento P, Marcie S, Lagrange JL, *et al.* Sequence-dependent effects of ZD1839 ('Iressa') in combination with cytotoxic treatment in human head and neck cancer. *Br J Cancer* 2002; 86:819–827.
23 Magne N, Fischel JL, Dubreuil A, Formento P, Poupon MF, Laurent-Puig P, *et al.* Influence of epidermal growth factor receptor (EGFR), p53 and intrinsic MAP kinase pathway status of tumour cells on the antiproliferative effect of ZD1839 ('Iressa'). *Br J Cancer* 2002; 86:1518–1523.
24 Xu JM, Azzariti A, Colucci G, Paradiso A. The effect of gefitinib (Iressa, ZD1839) in combination with oxaliplatin is schedule-dependent in colon cancer cell lines. *Cancer Chemother Pharmacol* 2003; 52:442–448.
25 Xu JM, Azzariti A, Severino M, Lu B, Colucci G, Paradiso A. Characterization of sequence-dependent synergy between ZD1839 ('Iressa') and oxaliplatin. *Biochem Pharmacol* 2003; 66:551–563.
26 Herbst RS, Giaccone G, Schiller JH, Natale RB, Miller V, Manegold C, *et al.* Gefitinib in combination with paclitaxel and carboplatin in advanced non-small-cell lung cancer: a phase III trial—INTACT 2. *J Clin Oncol* 2004; 22:785–794.
27 Gamboa-Dominguez A, Dominguez-Fonseca C, Quintanilla-Martinez L, Reyes-Gutierrez E, Green D, Angeles-Angeles A, *et al.* Epidermal growth factor receptor expression correlates with poor survival in gastric adenocarcinoma from Mexican patients: a multivariate analysis using a standardized immunohistochemical detection system. *Mod Pathol* 2004; 17:579–587.
28 Kopp R, Rothbauer E, Ruge M, Arnholdt H, Spranger J, Muders M, *et al.* Clinical implications of the EGF receptor/ligand system for tumor progression and survival in gastrointestinal carcinomas: evidence for new therapeutic options. *Recent Results Cancer Res* 2003; 162:115–132.
29 Perez-Soler R. HER1/EGFR targeting: refining the strategy. *Oncologist* 2004; 9:58–67.

Reprinted from:

9th Central European Lung Cancer *Conference*

Gdańsk (Poland), September 23-25, 2004

Editor

Jacek Jassem

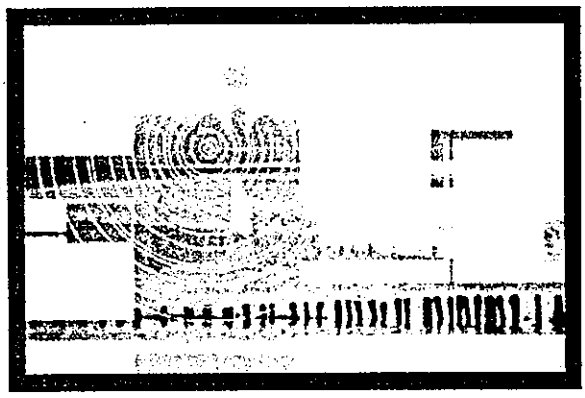

MEDIMOND

INTERNATIONAL PROCEEDINGS

Translational research for lung cancer – An update

K. Nishio[1], S. Korfee[1,2], W. Eberhardt[2], N. Saijo[1], and T. Tamura[1]

[1]*Shien-Lab, Medical Oncology, National Cancer Center Hospital and Pharmacology Division, National Cancer Center Research Institute, Tokyo, Japan.*
[2]*Department of Internal Medicine, West German Cancer Centre, Essen, Germany*

Correlative studies at the National Cancer Center Hospital

Molecular correlative studies are essential for the development of anti-cancer molecular target drugs. One of the major purposes of a correlative study is "proof of principle" (POP). However, clinical POP studies for small molecules are usually more difficult to complete than POP studies for antibodies[1].

Since 2001, the National Cancer Center Hospital (Tokyo, Japan) has been operating as a laboratory for translational studies to develop molecular correlative studies. The laboratory members consist of medical oncologists, basic researchers, CRC research fellows, invited researchers from abroad, technicians, and statisticians. The laboratory is located next to the phase I wards in the hospital, enabling more than ten molecular correlative studies to be simultaneously performed. New clinical samples can be quickly obtained from patients (including outpatients), prepared for storage, and stored in the laboratory. The medical doctors working in the laboratory are often research fellows supported by government grants, since these individuals are often interested in this kind of research.

The location of the laboratory also gives medical oncologists the opportunity to frequently communicate with research members. The significance of study endpoints, study designs, technical and statistical information, and feasibility are frequently discussed, especially among young medical oncologists and researchers. As a result, young oncologists and researchers often collaborate in the proposal of new molecular correlative studies.

The major activities of the laboratory are pharmacokinetics or pharmacodynamics studies for early clinical studies (PI and PII) and reverse translational studies. Tissue banking and quality control are two of the most important activities. Part of the clinical sample testing is performed in collaboration with the CRO.

Gene expression profiles

Gene expression arrays (DNA chips) have already been used in clinical studies to predict response and in POP studies. Many kinds of DNA chips are now available. Oligonucleotide arrays containing more than 40,000 genes have recently become popular. These chips can be used differentially, depending upon the study's purpose. Before clinical use, however, an array's quality (linearity and reproducibility) should be determined in preclinical studies. At our center, the quality of each array is evaluated and expressed as the Pearson's product-moment coefficient of correlation. Based on the validated quality of the cDNA, protocols based on "experienced designs" are then established.

In clinical settings, sample quality and feasibility are often major limitations in the design of new studies. To maintain the quality of clinical samples, a system for sample flow has been established. First the purity of the nucleotides must be carefully examined. Purification methods largely depend on the tumor types. For example, brain tumors contain large amounts of carbohydrate chains, lung cancer samples are sometimes very hard, and breast cancer biopsy samples are lipid rich. These sample characteristics influence purification quality and efficiency.

After the gene expression profiles have been obtained for each samples, the data is analyzed using standardization, clustering, statistical analysis, and validation methods. Statistical and biological validation is essential. Ideally, clinical cross-validation studies should be performed for independent clinical studies. On the other hand, biomarkers can be validated in the same clinical study using the "leave-one out" method. The endpoint of these correlative studies is usually the selection of biomarkers for predicting response or toxicity. For such endpoints, the quality of the clinical study itself is also very important.

We have also used another endpoint in early clinical studies. We compared the clinical samples obtained before and after treatment. Analysis of gene alterations after treatment can be utilized for POP. We completed these correlative studies as part of clinical studies for multitarget tyrosine kinase inhibitors, farnesyl transferase inhibitor, and cytotoxic drugs.

For biological confirmation, we usually perform (semi-)quantitative RT-PCR or immunostaining. However, we recently discovered that "pathway analysis" is a powerful method for improving our understanding of the alteration of genes related to biological signal transduction

pathways. For the analysis of transcription factors, "network analysis" can be used to identify the signaling pathways of the transcription factors.

Correlative Study for TKI using New Array

We have several developed new arrays in collaboration with biocompanies as follows;.

Fiber Array To differentially identify the isotypes of target genes, such as beta-tubulin, we have developed a customized, highly quantitative "fiber array" for "antimitotic inhibitors". We will analyze the isotype-specific expression profile of beta-tubulin using this array.

Genotyping Array Recently, the EGFR mutation has become an exciting topic in research on tyrosine kinase inhibitors (TKI). Mutation analysis is now essential for any correlative studies for TKI. Patients with tumors containing the EGFR mutation in different exons are thought to have different responses to TKI[2, 3]. Whole exon (and intron) analysis can now be performed using the chip technology available in our laboratory. Additional mutations after treatment are also generating interest with regard to their role in acquired resistance to TKI.

Arrays for proteins Proteomics technology has been developed and successfully used to identify biomarkers for target-based drugs in a few clinical studies. Additional approaches, such as antibody arrays and "power blots", especially those using phospho-specific antibodies, should enable us to perform "kinome" analyses. Thus, these protein analysis technologies are now powerful tools for research on tyrosine kinase inhibitors.

References

1. Saijo N, Nishio K, Tamura T. Translational and clinical studies of target-based cancer therapy. *Int J Clin Oncol* 2003;8:187-92.0
2. Lynch TJ, Bell DW, Sordella R, Gurubhagavatula S, Okimoto RA, Brannigan BW, Harris PL, Haserlat SM, Supko JG, Haluska FG, Louis DN, Christiani DC, Settleman J, Haber DA. Activating mutations in the epidermal growth factor receptor underlying responsiveness of non-small-cell lung cancer to gefitinib. *N Engl J Med* 2004;350:2129-39.0
3. Paez JG, Janne PA, Lee JC, Tracy S, Greulich H, Gabriel S, Herman P, Kaye FJ, Lindeman N, Boggon TJ, Naoki K, Sasaki H, Fujii Y, Eck MJ, Sellers WR, Johnson BE, Meyerson M. EGFR mutations in lung cancer: correlation with clinical response to gefitinib therapy. *Science* 2004;304:1497-500.0

Volume ISBN 88-7587-086-1
CD ISBN 88-7587-087-X

MEDIMOND S.r.l.

MONDUZZI EDITORE
INTERNATIONAL PROCEEDINGS DIVISION

Via Maserati 5, 40128 Bologna, Italy
Tel. (+39) 051 4151123 - Fax (+39) 051 370529
www.medimond.com

Int. J. Cancer: **108**, 679–685 (2004)

UICC Publication of the International Union Against Cancer

hnRNP L ENHANCES SENSITIVITY OF THE CELLS TO KW-2189

Fumiko TAGUCHI[1,3], Hitoshi KUSABA[1], Akira ASAI[4], Yasuo IWAMOTO[1], Keiichi YANO[4], Hirofumi NAKANO[4], Tamio MIZUKAMI[4], Nagahiro SAIJO[2], Harubumi KATO[3] and Kazuto NISHIO[1]*

[1]*Pharmacology Division, National Cancer Center Research Institute, Tokyo, Japan*
[2]*Medical Oncology Division, National Cancer Center Hospital, Tokyo, Japan*
[3]*Department of Surgery, Tokyo Medical University, Tokyo, Japan*
[4]*Tokyo Research Laboratories, Kyowa Hakko Kogyo Co. Ltd, Tokyo, Japan*

Heterogeneous nuclear ribonucleoproteins (hnRNPs) are involved in several RNA-related biological processes. We demonstrated hnRNP L as a candidate protein of DARP (duocarmycin-DNA adduct recognizing protein) by gel shift assay and amino acid sequencing. Stable transfectants of hnRNP L showed high sensitivity of the cells to the growth inhibitory effect of KW-2189, a duocarmycin derivative *in vitro*. Immunostaining of hnRNP L demonstrated differential intracellular localization of hnRNP L among human lung cancer cell lines. A transfection study using a series of deletion mutants of hnRNP L fused to indicated that the N-terminal portions of RRM(RNA recognition motif)1, RRM3 and RRM2 are involved in localization of hnRNP L. We identified sequences in these portions that have high homology with the sequences of known NLS (nuclear localization signal) and NES (nuclear export signal). hnRNP L is a factor that determines the sensitivities of cancer cells to the minor groove binder, and overexpression and differential intracellular localization of hnRNP L are involved in its function in lung cancer.

Key words: *hnRNP L; KW-2189; duocarmycin; minor groove binder; nuclear localization signal*

Heterogeneous nuclear ribonucleoproteins (hnRNPs) participate in a variety of processes involving RNA, including transcription, splicing, processing, translation and turnover, and there are approximately 20 major members of the hnRNP family.[1] High expression of some of these have been reported in several human malignant tumors and interest in the action of these proteins in malignancies has been growing.[2,3] HnRNP L is 68 kDa protein with 4 RNA recognition motifs (RRM). There have been several interesting reports demonstrating that cytoplasmic hnRNP L specifically interacts with VEGF mRNA in hypoxic cells *in vivo*, regulates VEGF mRNA stability[4] and binds in a sequence-specific manner to a *cis*-acting RNA sequence element that enables intron-independent gene expression.[5] The role of hnRNP L, however, still requires further study.

KW-2189 is a water-soluble derivative of antitumor antibiotic duocarmycin (DUM),[6–8] and DUM and its derivatives have been reported to exert their anti-tumor activity through covalent binding to the DNA minor groove and inhibition of DNA synthesis. We identified previously a nuclear protein DARP (duocarmycin-DNA adduct recognizing protein) in human cervical carcinoma HeLa S3 cells.[9] We purified the DARP from nuclear extract of HeLa S3 and its amino acid sequence was identical to hnRNP L. We investigated this, particularly in cancer cells.

MATERIAL AND METHODS

Cell cultures and reagents

Human small cell lung cancer cell lines SBC-3 and H69, human non-small cell lung cancer cell lines PC-14, and their respective cisplatin-resistant cell lines (SBC-3/CDDP, H69/CDDP,[10] and PC-14/CDDP[11]) were maintained in RPMI 1640 (Sigma, St. Louis, MO) supplemented with 10% heat-inactivated FBS (Gibco BRL, Gaithersburg, MD). Murine fibroblast cell line NIH3T3 and sublines (including cDNA transfectants) were cultured in DMEM (Nissui Pharmaceutical Co. Ltd., Tokyo, Japan) supplemented with 10% FBS. KW2189 was provided by Kyowa Hakko Kogyo Co., Ltd. A monoclonal antibody specific for hnRNP L (4D11) was generously provided by Dr. G. Dreyfuss (University of Pennsylvania, Philadelphia).

Cell extracts

Cells were washed twice with cold PBS and lysed in buffer (10 mM Tris-HCl pH 7.8, 1% Nonidet P-40, 0.15 M NaCl, 1 mM EDTA, 10 μg/ml aprotinin, 0.5 μg/ml leupeptin, 1 mM phenylmethane-sulfonyl fluoride [PMSF], 1 tablet/50 ml φgrComplete™ and 10% glycerol) for 60 min on ice. The lysates were centrifuged at 8,000*g* for 20 min, and supernatants were obtained as total protein. Protein concentration was measured by bicinchoninic acid protein assay (Pierce, Rockford, IL).

SBC-3, PC-14 and H69 cells were lysed in buffer A containing 10 mM HEPES-KOH (pH 7.9), 10 mM KCl, 0.1 mM EDTA-NaOH (pH 8.0), 0.1 mM ethyleneglycol bis(2-aminoethyl ether) tetraacetic acid (EGTA), 1 mM dithiothreitol (DTT), 0.5 mM PMSF, 1 mM aprotinin, and leupeptin. Nonidet P-40 (final concentration 0.5%) was added after allowing to stand on ice for 15 min. The supernatant obtained by centrifugation at 7,000*g* for 30 sec after standing on ice for 5 min was collected as the cytoplasmic fraction. The pellet was resuspended with buffer A containing 0.25 M sucrose, and after buffer B′ (buffer A containing 0.6 M sucrose) was added, the solution was centrifuged at 5,000*g* for 1 min at 4°C. The nuclei, which were contained in the pellet, were sonicated in buffer C containing 20 mM HEPES-KOH (pH 7.9), 0.4 M NaCl, 1 mM EDTA-NaOH (pH 8.0), 1 mM EGTA, 1 mM DTT and 1 mM PMSF, and then rocked at 4°C for 30 min and centrifuged at 8,000*g* for 10 min. The supernatant was used as the nuclear fraction. The nuclear protein content was adjusted to 5 μg per well, and the same volume of cytoplasmic protein was applied to the next well. The cytoplasmic and nuclear fractions were subjected to SDS-PAGE and Western blotting with anti-hnRNP L antibody.

Western blotting

An INSTA-Blot human tissues membrane (Imgenex, San Diego, CA), which contains 10 μg per lane of different human tissue lysates, was soaked in 100% methanol and then washed with TBST. After blocking the membrane in 5% skim milk in TBST for 1 hr at room temperature, it was probed with anti-hnRNP L antibody diluted (1:500) in TBST with 1% skim milk for 1 hr at

Fumiko Taguchi is a recipient of Research Resident Fellowship from the Foundation for Promotion of Cancer Research in Japan

*Correspondence to: Pharmacology Division, National Cancer Center Research Institute, 5-1-1 Tsukiji, Chuo-ku, Tokyo 104-0045, Japan. Fax: +81-3-3547-5185. E-mail: knishio@gan2.res.ncc.go.jp

Received 16 September 2002; Revised 25 August 2003; Accepted 12 September 2003

DOI 10.1002/ijc.11616
Published online 7 November 2003 in Wiley InterScience (www.interscience.wiley.com).

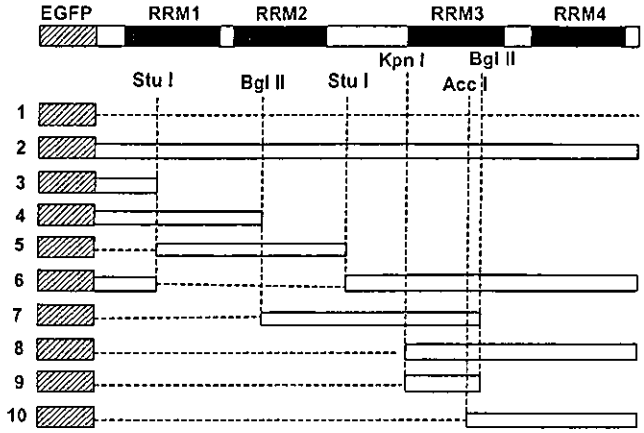

FIGURE 1 – Diagram of EGFP-hnRNP L deletion mutants. Known motifs, RNA recognition motifs (RRMs) 1, 2, 3 and 4 are boxed. The dark gray box denotes EGFP. Ten plasmids containing various parts of hnRNP L were constructed. The restriction sites used to generate deletion mutants are indicated.

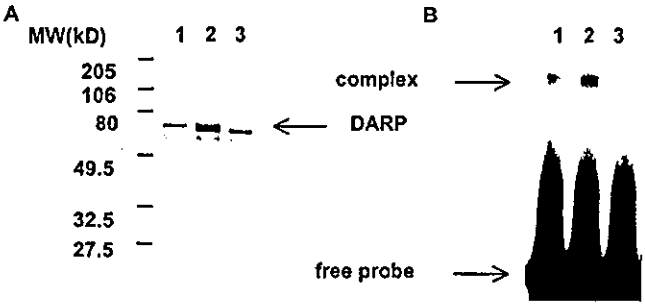

FIGURE 2 – Purification of DARP. (*a*) SDS-PAGE analysis of DEAE-sephacel fractions. *Lane 1*, 0.15 M KCl eluate; *Lane 2*, 0.2 M KCl eluate; *Lane 3*, 0.25 M KCl eluate. (*b*) Gel mobility shift assay of DEAE-sephacel fractions. *Lane 1*, 0.15 M KCl eluate; *Lane 2*, 0.2 M KCl eluate; *Lane 3*, 0.25 M KCl eluate. The oligonucleotides used as a probe contains the 5'-ATTA-3' sequence recognized by DUMSA (5'-GATC-CGGGATTACGATCGGGAGTCCCAGATTACGGCACCT-3'). The duplex oligonucleotides was incubated with each eluate after treatment with DUMSA as described in Material and Methods.

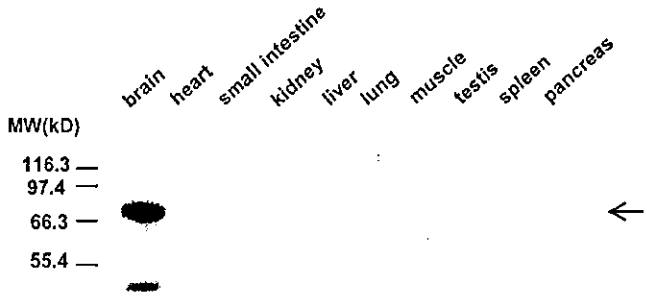

FIGURE 3 – Expression of hnRNP L in human tissues. Western blot analysis was carried out with anti-hnRNP L antibody. The membrane (INSTA-Blot) contains 10 μg per lane of different human tissue lysates. The arrow points to the hnRNP L protein.

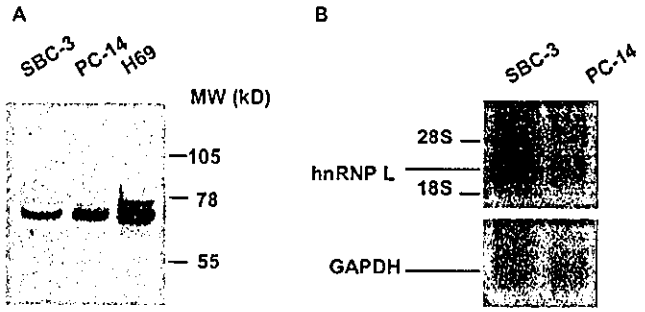

FIGURE 4 – Expression of hnRNP L in human lung cancer cell lines. (*a*) Cell lysates were prepared from 3 human lung cancer cell lines, separated with 7.5% SDS-PAGE, transferred to a membrane, and probed with anti-hnRNP L antibody. (*b*) Northern blotting was carried out with the 1030 bp fragment from hnRNP L cDNA as the probe.

room temperature, washed 3 times in TBST, incubated with anti-mouse IgG horseradish peroxidase antibody diluted (1:5000) in TBST with 1% skim milk for 1 hr at room temperature, and then washed 3 times in TBST. The signal was visualized with ECL (Amersham Pharmacia Biotech UK Ltd., Buckinghamshire, England), and Hyperfilm-MP (Amersham) was exposed to it.

Purification of DARP and amino acid sequencing

Purification of DARP was conducted as described previously.[9] DARP was detected by its ability to bind to DUMSA (one of DUMs)-DNA adduct in gel shift assays. Nuclear and cytoplasmic extracts from HeLa S3 cells (ATCC: American Type Culture Collection) were prepared according to previously published procedures. For identification of the DARP band, the aliquot of this material was subjected to DEAE-sephacel column again, and eluted with 0.5M stepwise procedure (0.1–0.5 M KCl) to give the small amount of purified DARP. Protein concentrations were estimated using Bio-Rad protein assay and the quality of the each fraction was checked by CBB (Coomassie brilliant blue) or silver staining of SDS-polyacrylamide gels. For analysis of amino acids sequence of DARP about 2 μg of affinity purified DARP was separated by 12% SDS-PAGE. The 60 kDa protein band was excised and digested with lysyl endopeptidase (WAKO, Japan) in 0.1 M Tris-HCl (pH 9.0), 4 M urea at 37°C for 16 hr. The resulting peptides were isolated by reversed phase HPLC on a RPC C2/C18 column (Amersham Pharmacia Biotech, Sweden). The amino acid sequence was determined by automated Edman degradation using a PPSQ-10 protein sequencer (Shimadzu, Japan).

Gel mobility shift assay

Labeled oligonucleotide (1 μg) was incubated with cell extract (final protein concentration, 20 μg/μl) at 30°C for 30 min in the presence of 2 μg of poly[dIdC]poly[dIdC] and 1 μg of BSA, except where stated, in a final volume of 15 μl of 0.1 M KCl HEDG. Where indicated, drug modified or unmodified calf thymus DNA was added to the reactions. Samples were electrophoresed in 6% polyacrylamide gel, dried and scanned.

Stable transfectants

Total RNA was prepared from HeLa cells with ISOGEN (Nippon Gene, Tokyo, Japan), and 14–784 and 636—1718 fragments of hnRNP L (2033 bp) were obtained by reverse transcription-polymerase chain reaction (RT-PCR). The PCR products were cloned in PCR II, a TA cloning plasmid vector, and then coupled at the Bcl I site. Subsequently, a fragment including hnRNP L was digested from the plasmid with Not I, and it was informed into the Not I site of the pRc/CMV vector. After confirming its sequence, this expression vector, pRc/CMV, containing cDNA of hnRNP L, was transfected into NIH3T3 cells with the Lipofectin reagent (Gibco BRL) according to the manufacturer's instructions. After 48 hr incubation, 1.5 mg/ml of G418 (Sigma) was added. Cells resistant to neomycin were selected, and isolated by limiting dilution methods.

Northern blotting

Total RNAs were prepared from SBC-3, PC-14 and NIH3T3 cells, and the 10 stable transfectants described above with ISO-

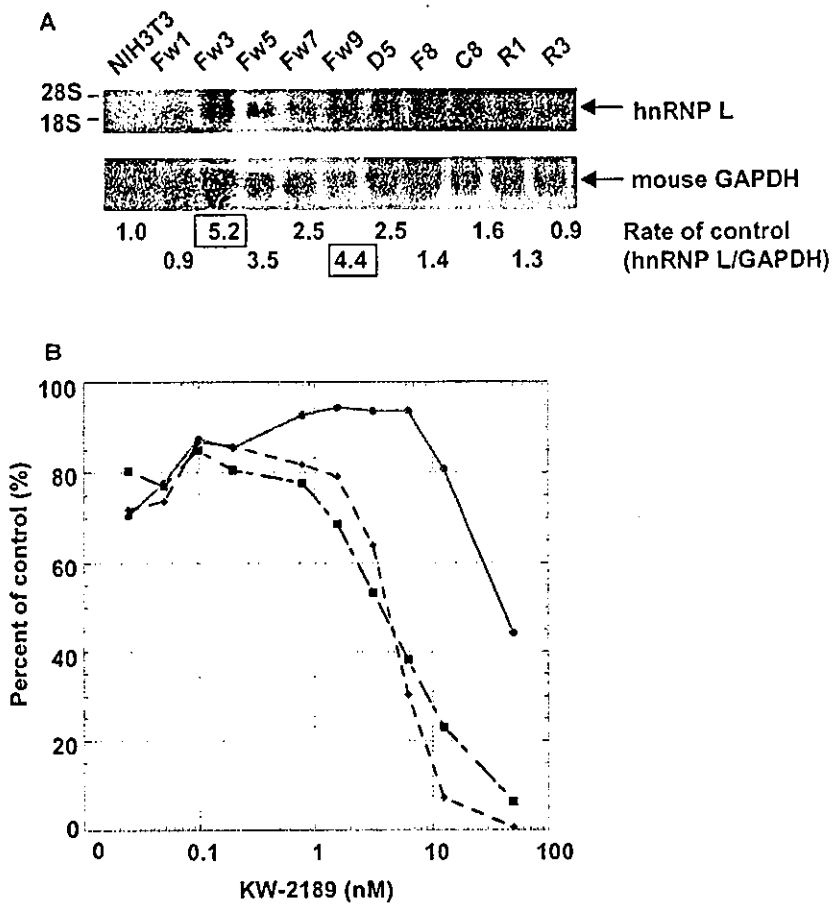

FIGURE 5 – Effect of hnRNP L on drug sensitivity. (*a*) Expression of hnRNP L mRNA in stable transfectants. Fw3 and Fw9 were chosen for the sensitivity tests. (*b*) MTT assay (KW-2189). C4 mock (●), Fw3 (■), Fw9 (□).

GEN reagent. RNA (12 μg) was electrophoresed and transferred to a positively charged nylon membrane (Hybond-N+). The 1030 bp fragment of hnRNP L cDNA was labeled with [α^{32}P]-dCTP by using the Rediprime II random primer labeling system (Amersham) and was used as a probe. The membrane was hybridized at 42°C overnight for blocking with sonicated salmon sperm DNA (Stratagene, La Jolla, CA) and hybridized at 42°C overnight with the labeled probe rotating. Washings were carried out in 2× SSC, 0.1% SDS, for 10 min at room temperature, 1× SSC, 0.1% SDS, for 1 hr at 42°C, and 0.2× SSC, 0.1% SDS, at 42°C for 1 hr. A BAS imaging plate (Fuji Photo Film Co. Ltd., Kanagawa, Japan) was exposed to the filter for 2 hr, and relative band intensities were measured with a BAS 2000 system (Fuji).

Growth-inhibition assay

The effect of hnRNP L on cell sensitivity to KW2189 was estimated by the 3-(4,5-dimethylthiazol-2yl)-2,5-diphenoyltetrazoliumbromide (MTT) assay. NIH3T3, and stable transfectants of hnRNP L cDNA, Fw3and Fw9 cells were exposed to 0–50 nM KW2189 for 72 hr before measuring absorbance. The OD values at 562–630 nm were measured with a 96-well microtiter plate reader, EL340 (Bio-Tek, Winooski, VT).

Immunochemical cell staining

Human lung cancer cell lines, SBC-3, PC-9, PC-14 and H69 cells were prepared on slide glasses with cytospin (Shandon, Pittsburgh, PA). The cells were dried and then fixed in cold acetone for 2 min. All of the incubation steps were carried out at room temperature, and Step 2 and 3 were carried out in the dark. The steps included: 1) incubation with 10% horse serum for 30 min for blocking; 2) incubation with anti-human hnRNP L (1:500 diluted in PBS with 1.5% blocking serum) for 60 min; and 3) incubation with fluorescence anti-mouse IgG (1:500 diluted) for 45 min. Slides were washed with 3 changes of PBS between each step. After Step 2 each washing was carried out for 5 min. The slides were mounted with 90% glycerol in PBS and examined with a fluorescence microscope (Nikon, Tokyo, Japan), equipped with fluorescein isothiocyanate filter set B-2A (Nikon).

EGFP-hnRNP L deletion mutants

pRc/CMV containing the 14–1718 fragment of hnRNP L cDNA (2033bp) was constructed as described above. After digesting the plasmid with SacII and BamHI, and the resulting fragment was introduced into the SacII/BamHI site of the pEGFP-C3 vector (Clontech, Palo Alto, CA), with the Takara DNA ligation system. Construction of deletion plasmids was carried out as follows. EGFP-hnRNP L (Construct 2) was partially digested with StuI and self-ligated to generate Constructs 3 and 6. PEGFP-hnRNP L was digested with BglII, and after extracting the 570 bp and 1023 bp fragments with a QIAquick Gel Extraction Kit (Qiagen, Hilden, Germany), each fragment was inserted into the BglII site of the pEGFP-C2 and -C3 vectors to generate Constructs 4 and 7, respectively. The 384 bp fragment of hnRNP L extracted by digesting with StuI was inserted into the SmaI site of pEGFP-C3 vectors to generate Construct 5. PEGFP-hnRNP L was digested with KpnI, and it self-ligated to generate Construct 8. The 584 bp fragment digested with KpnI and BglII and extracted was inserted into the BglII site of pEGFP-C3 vectors to generate Construct 9, and the 626 bp fragment digested with AccI was inserted into the AccI site of pEGFP-C3 vectors to generate Construct 10 (Fig. 1).

A cover-glass was placed on the bottom of each well of a 6-well culture dish, and each well was seeded with 1.6×10^5 NIH3T3 cells and incubated for 48 hr at 37°C. After diluting 2.5 μg/well of plasmid

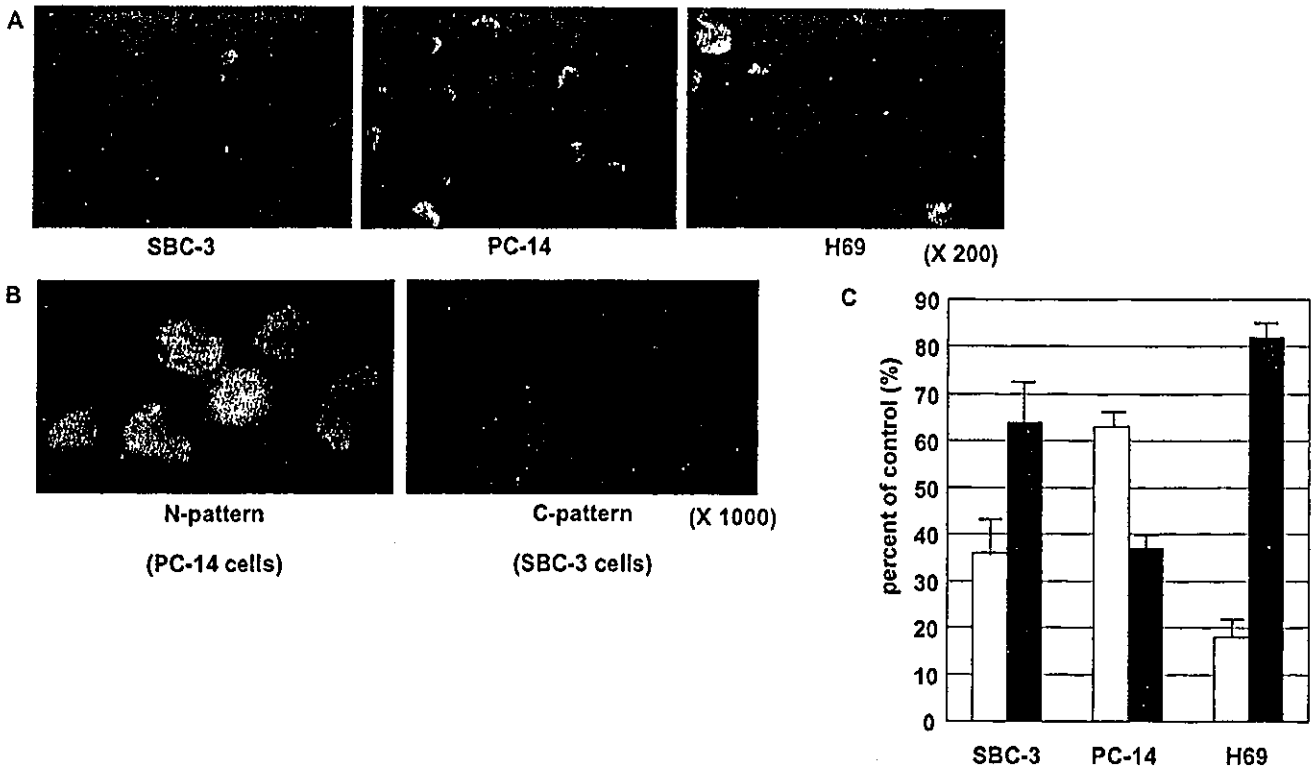

FIGURE 6 – Immunochemical staining of hnRNP L in human lung cancer cells. (*a*) Immunochemical cell staining was carried out using anti-hnRNP L antibody as the primary antibody and fluorescent anti-mouse IgG as the secondary antibody. (*b*) Intracellular localization of hnRNP L. (*c*) Cells were classified into N (white column) or C (gray column) patterns. Three independent cell counts were carried out.

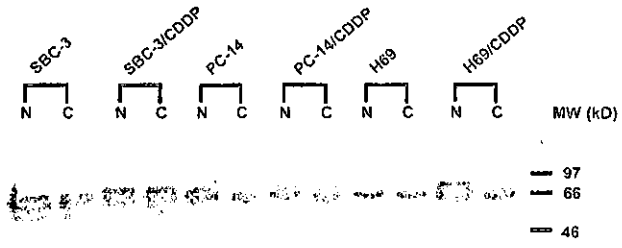

FIGURE 7 – Intracellular expression of hnRNP L in human lung cancer cell lines. The nuclear (N) and cytoplasmic (C) fractions of the cells were isolated as described in Material and Methods. Western blot analysis was carried out using anti-hnRNP L antibody. The cisplatin-resistant sublines were also examined to determine whether the localization patterns depended on the cell type.

DNA (pEGFP vectors containing deletion mutants of hnRNP L described above) in 1 ml/well of serum-free DMEM, 7.5 μl/well of 1 mM TransFast Reagent (Promega, Madison, WI) was added to the mixture. After allowing the mixture to stand for 15 min at room temperature, it was added to cells from which the growth medium was removed. The cells were then incubated for 1 hr at 37°C, and 1 ml/well of complete growth medium was added to them. At 24 hr after transfection, the cells were mounted on slides with aqueous mounting medium and examined under a fluorescence microscope (Nikon, B-2A filter, Tokyo, Japan).

RESULTS

Purification and sequence analysis of the DARP

Purification of the DARP was conducted as described previously.[9] After affinity purification, 2 main proteins were detected in SDS-PAGE with silver staining. Further purification efforts with DEAE-sephacel column chromatography gave a single band of Mr ~60,000 with the binding activity to the labeled duocarmycin-modified oligonucleotides (Fig. 2*a*). Coincubation of duocarmycin-treated calf thymus DNA with the labeled probe and purified DARP resulted in the retarded band in the gel mobility shift assay (Fig. 2*b*). Competition experiment in the presence of 30 and 300 ng of calf thymus DNA-DUMSA adduct demonstrated that 300 ng adduct reduced the intensity of the band in our previous study.[9]

The 60 kDa protein separated by SDS-PAGE was excised and digested with lysyl endopeptidase. The resulting peptides were eluted, separated by reversed phase HPLC, and sequenced. Three partial amino acid sequences were obtained, AAAGGGGGGGRYYGGG, DFSESRNNRFSTPEQAA and SDALETLGFLN, which were found to completely match parts of the predicted human heterogeneous nuclear ribonucleoprotein L. Gel mobility shift assay using anti-hnRNP L did not, however, show the supershift of the band induced by anti-hnRNP L (data not shown).

Expression of hnRNP L

Western blot analysis was carried out using a membrane containing normal human tissue lysates from different organs. A 68 kDa band of hnRNP L was detected in total protein extracts from brain and small intestine, but not in others, including normal lung (Fig. 3). The expression of hnRNP L protein, however, was detected in the human lung cancer cell lines (Fig. 4*a*). Northern blot analysis confirmed the expression of hnRNP L at the mRNA (~2 kbp) level in these cells (Fig. 4*b*). In contradiction to our first result that hnRNP L was not detected in normal lung tissue, the expression of hnRNP L in malignant cells seemed to increase.

Effect of hnRNP L on drug sensitivity

To evaluate the function of hnRNP L, hnRNP L cDNA was transfected into NIH3T3 cells, and stable transfectant clones were

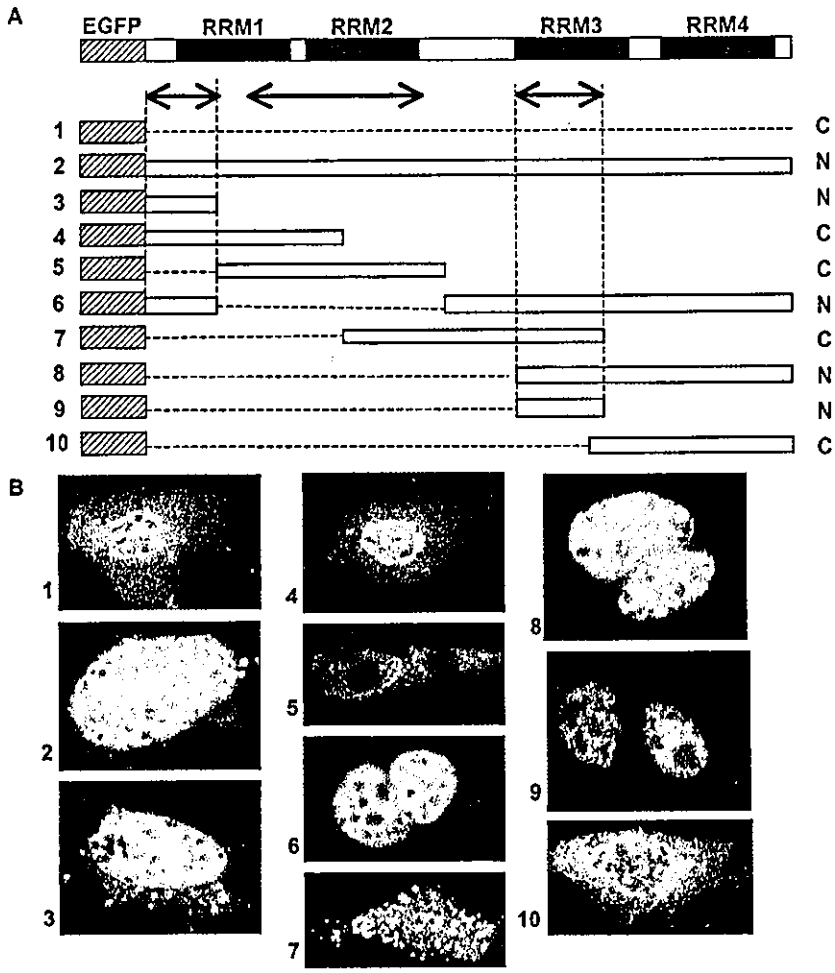

FIGURE 8 – Effect of hnRNP L deletion on the intracellular localization of EGFP-hnRNP L. (*a*) Arrows indicate the part expected to be responsible for localization of hnRNP L. Letters N (nuclear localization) and C (cytoplasmic localization) at the right end indicate the results of classification by the transfection study. (*b*) Localization of EGFP-hnRNP L deletion mutants. NIH3T3 cells were transfected with each construct, and they were examined by fluorescent microscopy to identify the localization of EGFP-fusion. The numbers correspond to those of the constructs in (*a*).

characterized. The Fw3 and Fw9 clones showed higher expression of hnRNP L mRNA than other transfectants by 5.2-fold and 4.4-fold to control respectively detected by Northern blot analysis (Fig. 5*a*).

We measured the growth inhibitory effect of KW-2189 in the hnRNP L transfectant cells by MTT assay. The IC_{50} values for KW-2189 in the Fw3 and Fw9 clones were 3.5 nM and 4.3 nM, respectively, and the Fw3 and Fw9 cells were 13.4-fold and 10.9-fold, respectively, more sensitive to KW-2189 than the Mock transfectant C4 cells (IC_{50}: 47 nM) (Fig. 5*b*). These results indicate that hnRNP L enhances cell sensitivity to the growth inhibitory effect of KW-2189 *in vitro*. We also examined the sensitivity of the transfectants to cisplatin and mitomycin C and no difference of the sensitivity was observed between the transfectants and the Mock cells (data not shown). The hnRNPs have been reported to regulate both nuclear and cytoplasmic events, as described above, and the intracellular localization of hnRNP L was examined in the next step to identify the site of action of hnRNP L in the sensitivity enhancement machinery.

Localization of hnRNP L protein in human lung cancer cell lines

We carried out immunofluorescence cell staining with anti-hnRNP L antibody to determine the subcellular localization of hnRNP L protein in human lung cancer cells (Fig. 6*a*). Based on the results, the localization of hnRNP L cells could be classified into two patterns: nuclear localization (N) and cytoplasmic localization (C) (Fig. 6*b*). As shown in Figure 6*c*, the cytoplasmic pattern was observed frequently in SBC-3 and H69 cells, whereas the nuclear pattern was common in PC-14 cells. To confirm this differential distribution, fractionated proteins from the nuclear and cytoplasmic fractions of these cells were immunoblotted with anti-hnRNP L antibody (Fig. 7). The results showed that hnRNP L was expressed equally in the nucleus and cytoplasm of the SBC-3 and H69 cells, whereas it was expressed predominantly in the nuclei of the PC-14 cells. These results are consistent with the immunocytological findings. In addition, the cisplatin-resistant sublines derived from these cells exhibited the same localization pattern as their parental cells. This indicates that the differential localization depends on the cell type.

Motifs required for the intracellular localization of hnRNP L

It has been reported that hnRNP L is localized in the nucleoplasm of HeLa cells, except the nucleoli,[12] but the mechanism of its localization remains unknown. To identify the motifs responsible for the localization of hnRNP L, we constructed an hnRNP L deletion series fused to EGFP (Fig. 8*a*), transfected the constructs into NIH3T3 cells, and examined them under a fluorescence microscope. As shown in Figure 8*b*, EGFP protein itself was rather evenly distributed throughout the cell, the cytoplasm and the nucleus (Transfectant 1). Full-length hnRNP L was present in the nucleoplasm, except the nucleoli (Transfectant 2). Deletion mutants containing the N-terminal portion of RRM1 or of RRM3 (Transfectants 3, 6, 8 and 9) showed hnRNP L localization in the nucleus. Transfectants 4, 5 and 7, containing the N-terminal portion of RRM2 showed hnRNP L distributed through the cell, whether they also contained that portion of RRM1 and RRM3 or not. In Transfectant 10, which lacked the N-terminal region of all